

Article

Theoretical and Cyclic Voltammetric Analysis of Asparagine and Glutamine Electrocatalytic Activities for Dopamine Sensing Applications

Gururaj Kudur Jayaprakash ^{1,*}, B. E. Kumara Swamy ², Roberto Flores-Moreno ³
and Kayim Pineda-Urbina ⁴

¹ Department of Chemistry, Nitte Meenakshi Institute of Technology, Bangalore 560064, India

² Department of P.G. Studies and Research in Industrial Chemistry, Kuvempu University, Shimoga 577451, India

³ Departamento de Química, Centro Universitario de Ciencias Exactas e Ingenierías, Universidad Guadalajara, Blvd. Marcelino García Barragán 1421, Guadalajara C.P. 44430, Jalisco, Mexico

⁴ Facultad de Ciencias Químicas, Universidad de Colima, Carr. Colima-Coquimatlán, km. 9, Coquimatlán C.P. 28400, Colima, Mexico

* Correspondence: rajguru97@gmail.com

Abstract: The molecular dynamics and density functional theory (DFT) can be applied to discriminate electrocatalyst's electron transfer (ET) properties. It will be interesting to discriminate the ET properties of green electrocatalysts such as amino acids. Here, we have used DFT to compare the electrocatalytic abilities of asparagine and glutamine at the carbon paste electrode interface. Cyclic voltammetric results reveal that the electrocatalytic activities of asparagine are higher than glutamine for dopamine sensing. Dopamine requires less energy to bind with asparagine when compared to glutamine. Additionally, asparagine has higher electron-donating and accepting powers. Therefore, asparagine has a higher electrocatalytic activity than glutamine—the ability for the asparagine and glutamine carbon electrodes to detect dopamine in commercial injection, and to obtain satisfactory results. As a part of the work, we have also studied dopamine interaction with the modified carbon surface using molecular dynamics.

Keywords: catalysts; analytical Fukui; DFT; redox



Citation: Kudur Jayaprakash, G.; Swamy, B.E.K.; Flores-Moreno, R.; Pineda-Urbina, K. Theoretical and Cyclic Voltammetric Analysis of Asparagine and Glutamine Electrocatalytic Activities for Dopamine Sensing Applications. *Catalysts* **2023**, *13*, 100. <https://doi.org/10.3390/catal13010100>

Academic Editors: Vera Bogdanovskaya and Inna Vernigora

Received: 10 November 2022

Revised: 25 December 2022

Accepted: 27 December 2022

Published: 3 January 2023



Copyright: © 2023 by the authors. Licensee MDPI, Basel, Switzerland. This article is an open access article distributed under the terms and conditions of the Creative Commons Attribution (CC BY) license (<https://creativecommons.org/licenses/by/4.0/>).

1. Introduction

Neurotransmitters are chemicals that are required for neuron transmission, and they play an important role in brain function. For neurobiology research and the development of innovative diagnostic and therapeutic techniques for brain illnesses impacting on neurotransmitter levels and dynamics, the precise sensing of neurotransmitter concentrations in the brain and real samples is critical [1,2]. Dopamine (3,4-dihydroxyphenethylamine) is an important neurotransmitter that regulates various physiological processes in the human brain and body, including motor function, memory, motivation, arousal, and reward. Abnormal changes in dopamine (DA) levels can have serious effects and are at the root of brain illnesses such as schizophrenia, anxiousness, Parkinson's disease, low sex drive, Alzheimer's disease, depression, and attention deficit hyperactivity disorder [3,4]. The capacity to identify physiologically appropriate DA concentrations in the brain or in brain-derived biological samples using high-throughput techniques can speed up the development of early diagnosis and effective therapies for these illnesses.

Traditional analytical methods for monitoring and detecting DA, such as enzyme-linked immunosorbent assays [5], colorimetric methods [6], nanoplasmonic probe [7], capillary electrophoresis [8], and spectroscopic methods (fluorescence, surface-enhanced Raman spectroscopy, magnetic resonance spectroscopy, infrared Fourier transform, and X-ray absorption spectroscopy) [9–12], depend on enlarged, high-priced equipment, or

they necessitate laborious sample preparation and long detection cycles. Electroanalytical techniques, particularly voltammetric methods based on DA sensing, provide various advantages, including rapid and extremely sensitive responses, are easily operated, and are inexpensive. Because DA is electroactive, determining it via electrochemical methods is a critical scientific challenge. Therefore, novel developing techniques have focused on tiny chemical sensors based mostly on catalytic and electrochemical processes, but they have largely lacked important selectivity and sensitivity [13–16]. Hence, selecting a suitable working electrode is crucial in the voltammetric detection of DA.

Carbon paste electrodes (CPEs) have been utilized as working electrodes in voltammetric sensing applications because they have a number of advantageous qualities, such as ease of preparation, stability for many cycles, repeatability, biocompatibility, and surface renewability. In general, the active electron transfer (ET) sites/kinetics of the bare CPE (BCPE) is quite low. As a result, the performance of the BCPE will not be up to mark for the sensor applications. Therefore, researchers are proposing modified CPE (MCPE) to overcome these difficulties [17–25].

The most simple MCPE can be prepared by spiking different modifiers such as inorganic compounds [13,26,27], organic moieties [28], plant extracts [29], ionic liquids [30], polymers [16], and nanomaterials [31–33] to the carbon paste. After the modification at the MCPE interface, the redox electron transfer (ET) event occurs between the modifiers and the analyte (DA) frequently, with a significant decrease in the activation overpotential. Here, it is interesting to note that activation overpotential is completely dependent on the structure of the modifiers [13–16]. In particular, an addition of the biocompatible modifiers to the carbon paste will be beneficial for futuristic biosensor applications. Amino acids are the most simple organic molecules, are readily available in chemistry laboratories, and they are compatible with human tissues. Therefore amino acids are the right choice for CPE modifications. CPE can be modified using amino acids by simply spiking them on the carbon paste or depositing them as electropolymers at the electrode interface. Preparing MCPE via spiking methods is advantageous because of the ease of preparation. In the case of electropolymer modification, amino acids may be deposited as dimers, trimers, or polymers. It will be interesting to compare the amino acids ET activities as an electrocatalyst at the MCPE interface.

Computational models based on the density functional theory (DFT) method are able to compare the global ET properties such as the electron-donating and electron-accepting powers of the different moieties [34–38], and electrocatalysts (modifiers) [13,14]. In particular, conceptual DFT-based frontier molecular orbital (FMO) and auxiliary density perturbation theory (ADPT)-based analytical Fukui functions are used to locate redox ET, and to mediate the processes of the electrocatalyst [13,14,39]. The pre-ET can be located from FMO, and post-ET using analytical Fukui functions.

Asparagine (ASP) and glutamine (GLU) are structurally similar amino acids (only a methylene group different). Therefore, we have selected ASP and GLU as electrocatalysts to modify the CPE. By pulverizing ASP and GLU separately in a pestle and mortar, we have fabricated the MCPE. Conceptual DFT-based computational modeling were used to predict the redox reactive sites and the mediating mechanisms of the ASP and GLU molecules. The FMO, the highest occupied molecular orbital (HOMO), and the lowest unoccupied molecular orbital (LUMO) densities are utilized to determine the nucleophilic and electrophilic regions of ASP and GLU. To support the findings, the outcomes of the FMO results were further assessed using analytical Fukui functions.

2. Experimentation

2.1. Reagents and Chemicals

We bought graphite powder from Loba Chemicals (Mumbai, India). The supporting electrolyte (sodium dihydrogen orthophosphate monohydrate and disodium hydrogen orthophosphate), GLU, silicone oil, ASP, and DA were purchased from Sigma-Aldrich Himedia (Bengaluru, India).

2.2. Fabrication of BCPE

The BCPE was manufactured by thoroughly hand mixing the binder (silicon oil) and carbon (graphite) powder in a pestle using an agate mortar and pestle for 40 min until the paste became uniform and homogeneous. Graphite powder and silicon oil in a 75:25 (*w/w*) ratio were rigorously mixed by hand for 25 min in an agate mortar with a pestle until the paste was uniform and homogeneous. Then, a Teflon tube with a 3 mm hole was filled with the graphite paste. For a uniform and clean surface, the electrode surface was gently rubbed on a soft tissue paper [13–16,40].

2.3. Fabrication of the ASP- and GLU-Modified Carbon Paste Electrodes

By manually grinding different concentrations of ASP and GLU with carbon paste using an agate mortar, ASP-MCPE and GLU-MCPE were fabricated as described in our previous work [17].

2.4. Electrochemical Setup

The CH-660 C potentiostat model (CH-Instruments, Inc., Bee Cave, TX 78738, USA) was used to perform the cyclic voltammetric (CV) experiments. A three-electrode cell was utilized, with the working electrodes (BCPE, ASP-MCPE, and GLU-MCPE) and a saturated calomel electrode (SCE) serving as the reference electrode, and a platinum rod serving as the counter electrode.

2.5. Computational Methods

To construct the model geometries, we utilized the Sinapsis program (Jalisco, Mexico) [41] and ADPT-based DFT calculations, as implemented in the deMon2k software (Mexico City, Mexico) [42,43], and BLYP [44,45] correlation functions; and the TZVP [46] basis set was used for computation. Sinapsis [41] was used to display the FMO (HOMO and LUMO) and analytical Fukui functions. Figure 1 depicts the theoretical models of ASP (Figure 1a) and GLU (Figure 1b).

Molecular dynamics conformational searches were run using the AMBER [47] potential as implemented in the Gabedit software (Lyon, France) [48], along with PM6 interactive minimizations via MOPAC (Beijing, P.R. China) [49]. Geometry optimizations were performed in ORCA 4.1.2 [50], with a combination of the PBE exchange-correlation functional and def2-SVP basis set. Dispersion corrections were included via the DFT-D3BJ method. CM5 partial atomic charges were computed in Multiwfn 3.8 software. Basis set superposition errors in binding energies were corrected using the counterpoise method. Water solvation effects were implicitly included through the SMD solvation model.

By applying the following formulas to the geometry-relaxed energies of the compounds (*N* electron system) with the corresponding *N* – 1 (reduced) and *N* + 1 (oxidised) electron systems, the following values of the compounds were determined: electron affinity (EA), ionization potential (IP), hardness (η), softness (*S*), electron-donating power (ω^-), electron-accepting power (ω^+), and Fukui functions.

$$EA(\text{compound}) = E(\text{reduced compound}) - E(\text{compound}) \quad (1)$$

$$IP(\text{compound}) = E(\text{oxidized compound}) - E(\text{compound}) \quad (2)$$

$$\eta = \frac{1}{2} \left(\frac{\partial \mu}{\partial N} \right)_v = \frac{1}{2} \left(\frac{\partial^2 E}{\partial N^2} \right)_v = \frac{1}{2} (IP - EA) \quad (3)$$

$$S = \frac{1}{2\eta} \quad (4)$$

$$\omega^- = \frac{(3IP + EA)^2}{16(IP - EA)} \quad (5)$$

$$\omega^+ = \frac{(IP + 3EA)^2}{16(IP - EA)} \quad (6)$$

$$f^{\pm}(\mathbf{r}) = \left(\frac{\partial \rho(\mathbf{r})}{\partial N} \right)_{v(\mathbf{r})}^{\pm} \quad (7)$$

Here, N is the total number of electrons in a molecule, $\rho(\mathbf{r})$ is electron density, and $v(\mathbf{r})$ is external potential. $+$ is the addition of electrons and $-$ is the removal of electrons.

3. Results and Discussion

3.1. CV Response of DA at GLU-MCPE

Five different GLU concentrations (2, 4, 6, 8, and 10 mg) were spiked onto the carbon paste to prepare GLU-MCPE as described in the methodology sections. Figure 2 shows CVs for 10 μM DA in 0.1 M PBS with a pH of 7.4 at BCPE (black line), and GLU-MCPE with varying amounts of GLU at a scan rate of 0.05 V/s. Table 1 compares the DA anodic peak current (i_{pa}) values for BCPE and GLU-MCPE with different amounts of GLU. According to Figure 2 and Table 1, GLU-MCPE with 4 mg of GLU had the highest i_{pa} value. The ΔE_p value of 0.54 V indicates that redox ET process is quasi-reversible.

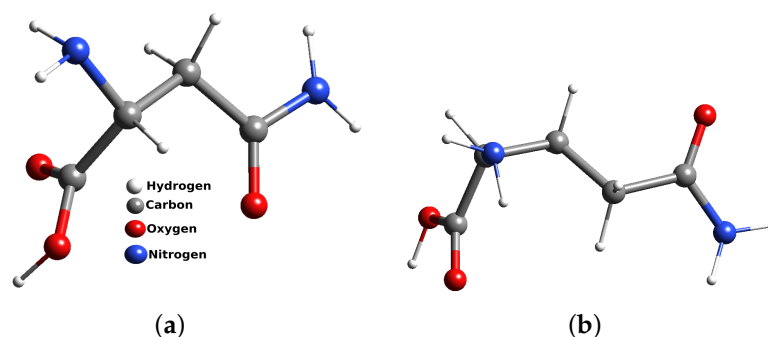


Figure 1. Computational models of ASP and GLU. (a) Asparagine; (b) Glutamine.

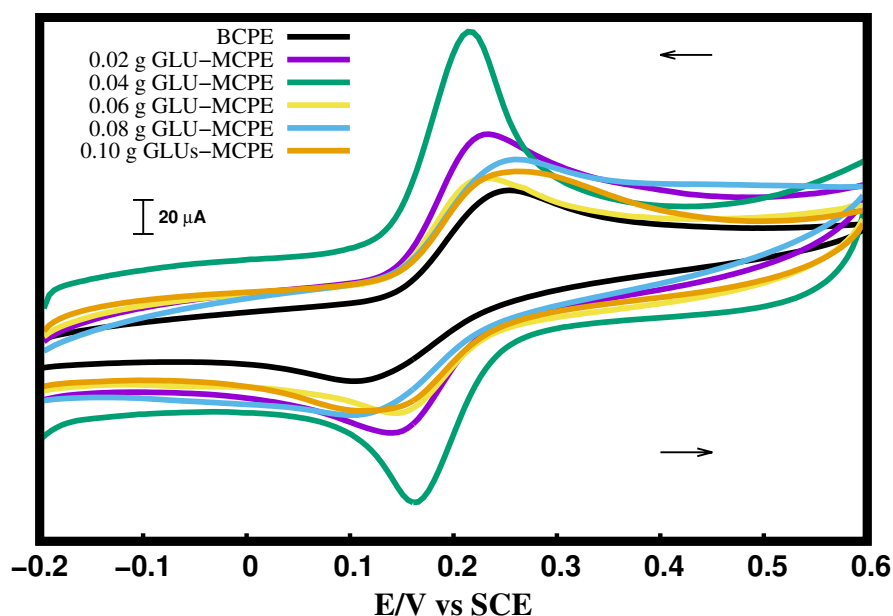


Figure 2. CV of 10 μM DA at BCPE and GLU-MCPE.

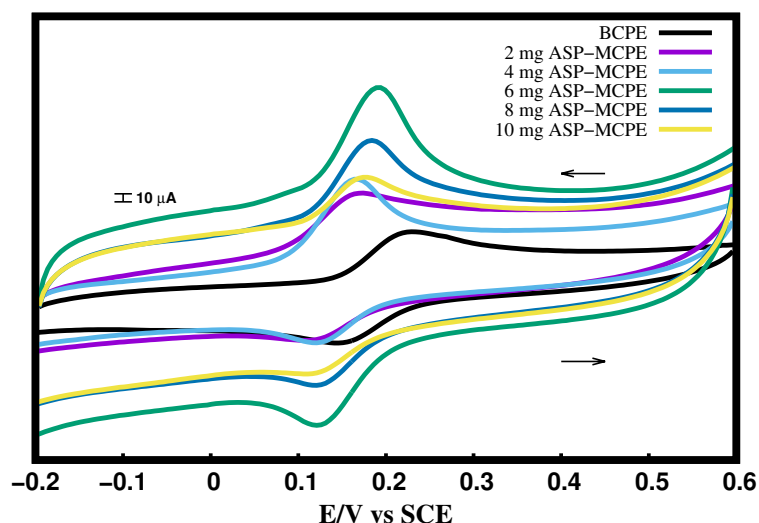
As a result, we chose 4 mg GLU-MCPE for further investigation.

Table 1. i_{pa} values of BCPE and GLU-MCPE with different quantities of GLU (data taken from Figure 2).

| El. No. | $i_{pa}/\mu\text{A}$ |
|-----------------|----------------------|
| BCPE | 76.129 |
| 0.02 g GLU-MCPE | 109.084 |
| 0.04 g GLU-MCPE | 169.567 |
| 0.06 g GLU-MCPE | 83.766 |
| 0.08 g GLU-MCPE | 94.124 |
| 0.10 g GLU-MCPE | 86.981 |

3.2. CV Response of DA at ASP-MCPE

The carbon paste was spiked with 2, 4, 6, 8, and 10 mg of ASP. Figure 3 shows cyclic voltammograms (CVs) for 10 μM DA in 0.1 M phosphate buffer solution (PBS) with a pH of 7.4 at BCPE (black line), and ASP-MCPE with different amounts of ASP at a scan rate of 0.05 V/s. In Table 2, the DA i_{pa} values for BCPE and ASP-MCPE with different amounts of ASP are compared. Figure 3 and Table 2 show that the i_{pa} value was highest for ASP-MCPE with 6 mg of ASP. The ΔE_p value of 0.34 V indicates that the redox ET process is reversible. Because of this, we chose 6 mg ASP-MCPE to study further.

**Figure 3.** CV of 10 μM DA at BCPE and ASP-MCPE.**Table 2.** i_{pa} values of BCPE and ASP-MCPE with different quantities of ASP (data taken from Figure 3).

| El. No. | $i_{pa}/\mu\text{A}$ |
|-----------------|----------------------|
| BCPE | 76.129 |
| 0.02 g ASP-MCPE | 133.387 |
| 0.04 g ASP-MCPE | 150.057 |
| 0.06 g ASP-MCPE | 267.924 |
| 0.08 g ASP-MCPE | 200.080 |
| 0.10 g ASP-MCPE | 155.013 |

3.3. Comparison of the DA Response at ASP-MCPE and GLU-MCPE

CV was used to compare the electrochemical performance of ASP-MCPE and GLU-MCPE for 10 μM DA in 0.1 M PBS with a pH of 7.4 at a scan rate of 0.05 V/s. Figure 4 shows

the CVs of ASP-MCPE and GLU-MCPE for DA sensing. In the specified potential range, DA demonstrates weak CV responses at GLU-MCPE, with an anodic peak potential (E_{pa}) of 0.216 V and a cathodic peak potential (E_{pc}) of 0.162 V. In the case of ASP-MCPE, the E_{pa} was shifted downward/negative (0.218 V to 0.192 V), while the E_{pc} remained almost the same (0.162 V to 0.158 V) with the higher redox peak currents than GLU-MCPE. The obtained CV responses indicate that ASP-MCPE outperforms GLU-MCPE as a DA electrochemical sensor. In terms of structure, ASP and GLU are nearly identical (with the exception of the methylene group). From the CV studies, it is clear that why ASP-MCPE show better electrocatalytic activity than GLU-MCPE. The lower ΔE_p values at ASP-MCPE and GLU-MCPE when compared to BCPE indicate that ASP and GLU modification are helpful for improving carbon electrode electron transfer properties. Based on our experience in computational electrochemistry, DFT-based quantum chemical models can help solve this molecular-level mystery.

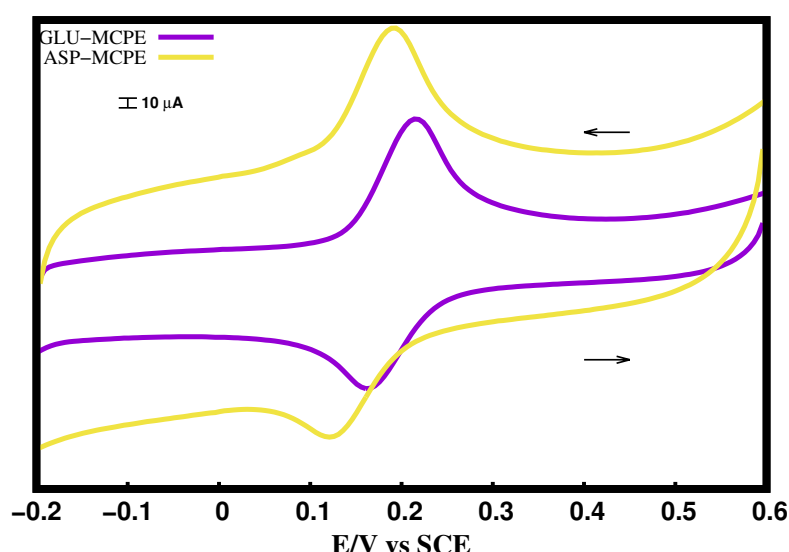


Figure 4. CV of 10 μM DA at ASP-MCPE and GLU-MCPE.

3.4. Global ET Properties of ASP and GLU

Figure 1 depicts the theoretical models of ASP (Figure 1a) and GLU (Figure 1b), and Table 3 lists their quantum chemical properties. From the Table 3, it is clear that the global ET properties of ASP are higher than the GLU. Therefore, the electrocatalytic activities of ASP are higher than GLU. We have also calculated the binding energies (B.E.) between the dopamine and the modifiers (ASP and GLU), as displayed in the Table 4. The B.E. was calculated using Equation (8)

$$\text{B.E.} = E_{\text{ASP/GLU-DA}} - (E_{\text{ASP/GLU}} + E_{\text{DA}}) \quad (8)$$

where $E_{\text{ASP/GLU-DA}}$, $E_{\text{ASP/GLU}}$, and E_{DA} are the ground state electronic energies of the optimized structure for the ASP/GLU-DA complex, ASP/GLU, and DA, respectively.

DA can bind more easily to ASP (requiring less B.E.) when compared to GLU. This may be also one of the reasons for the increased redox peak currents at ASP-MCPE when compared to GLU-MCPE.

Table 3. Global ET properties of ASP and GLU.

| SI/No. | Model | IP eV | EA eV | η eV | S eV | ω^- eV | ω^+ eV |
|--------|-------|----------|----------|--------------|---------|------------------|------------------|
| 1 | ASP | 8.076 | 0.403 | 3.836 | 0.130 | 4.941 | 0.702 |
| 2 | GLU | 8.008 | 0.748 | 3.630 | 0.137 | 4.664 | 0.286 |

Table 4. B.E. of ASP and GLU with DA.

| SI/No. | Model | B.E. eV | E_{pc} V | E_{pa} V | Δ_{EP} V |
|--------|-------|------------|---------------|---------------|--------------------|
| 1 | ASP | −0.163 | 0.128 | 0.192 | 0.064 |
| 2 | GLU | −0.0928 | 0.162 | 0.216 | 0.054 |

The CPE surface was represented by a graphene layer made of 150 carbon atoms saturated by hydrogen atoms on its edges for the molecular dynamics simulations shown in Figure 5. A single molecule of either ASP or GLU was added to complete the depiction of the electrochemically active sites of the sensor. In addition, a single molecule of DA was included to model the sensing interaction of the modified electrodes.

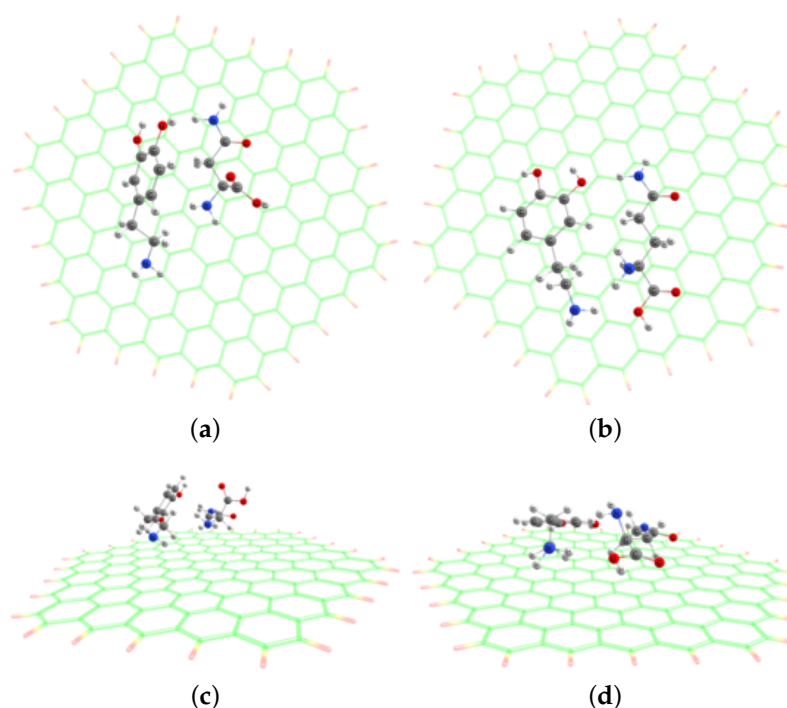


Figure 5. Optimized structures for DA-ASP-MCPE (a) and DA-GLU-MCPE (b) with alternative views on the bottom [DA-ASP-MCPE (c) and DA-GLU-MCPE (d)]. The carbon surface is represented as sticks for clarity's sake.

Optimized structures for DA-ASP-MCPE (left) and DA-GLU-MCPE (right), with alternative views on the bottom. The carbon surface is represented as sticks for clarity's sake.

DA takes a different conformation when interacting with ASP-MCPE and GLU-MCPE, respectively. While the aromatic ring faces the ASP portion in the DA-ASP-MCPE system, it faces the carbon surface in the case of DA-GLU-MCPE. Dopamine's binding energy was -1.59 eV in the case of DA-ASP-MCPE, and -1.86 eV for DA-GLU-MCPE. This suggests that the mass transfer process is slightly favored in the GLU-MCPE sensor. However, the DA partial charge is 0.068 a.u. in the case of DA-ASP-MCPE, while its charge is -0.065 a.u. for DA-GLU-MCPE. The DA-ASP-MCPE interaction seems to favor a charge transfer towards DA's oxidation, which is important as this is the electrochemical signal used in the experiment. This could account for ASP-MCPE's better performance as a DA sensor.

3.5. Local ET Properties (FMO and Analytical Fukui) of ASP and GLU

The electrocatalytic activities of CPE towards DA are increased when the modifiers (ASP and GLU) are physically bound on the surface of the graphite paste electrode. For

the purpose of mathematical modeling, a monomer of ASP and GLU is taken into account, as described in previous research works. In general, FMO can be employed to ascertain which atoms of the electrocatalyst are involved in the pre-ET processes.

Previously, we have modeled several amino acids such as lysine, glycine, serine, and alanine, and have used FMO and analytic Fukui functions to understand the roles of different functional groups such as amine, hydroxyl, and carboxylic acid in redox ET reactions. ASP and GLU are completely different to the above mentioned amino acids, because they have an amide group in addition to the amine and carboxylic acid groups. Therefore, it is interesting to understand the redox ET properties of amine and carboxylic acid of amino acids in the presence of an amide group.

Traditionally, electrochemists were employing the condensed Fukui function concept to locate the post-ET sites of the electrocatalysts. In contrast to the condensed Fukui functions, analytical Fukui functions based on auxiliary density perturbation theory (ADPT) have advantages such as being applicable to larger systems and having fewer human errors. Additionally, it will get rid of numerical method artifacts. As a result, in the current work, we employ analytical Fukui functions based on ADPT.

The FMO results of ASP and GLU are shown in Figure 6. ASP's HOMO is shown in Figure 6a. From Figure 6a, it is clear that the amine group and oxygen atom of the acetamide group act as oxidation centers, and as shown in Figure 6b, carboxylic acid group acts as a reduction center. GLU's HOMO is shown in Figure 6c; interestingly, in this case, the oxygen atom of the acetamide group acts as an oxidation center and the carboxylic group acts as the reduction center (shown in Figure 6d). When compared to ASP, the GLU carbonyl carbon atom of the amide group experiences a reduced negative inductive effect from the amine group. Therefore carbonyl oxygen's lone pair of electrons are easier to remove in case of GLU when compared to ASP. While the presence of two electronegative oxygen atoms on carboxylic carbon makes it more electron deficient, there, it acts as LUMO in both the molecules. Thus, the local ET descriptors obtained from conceptual DFT are able to discriminate the redox ET regioselectivities of ASP and GLU.

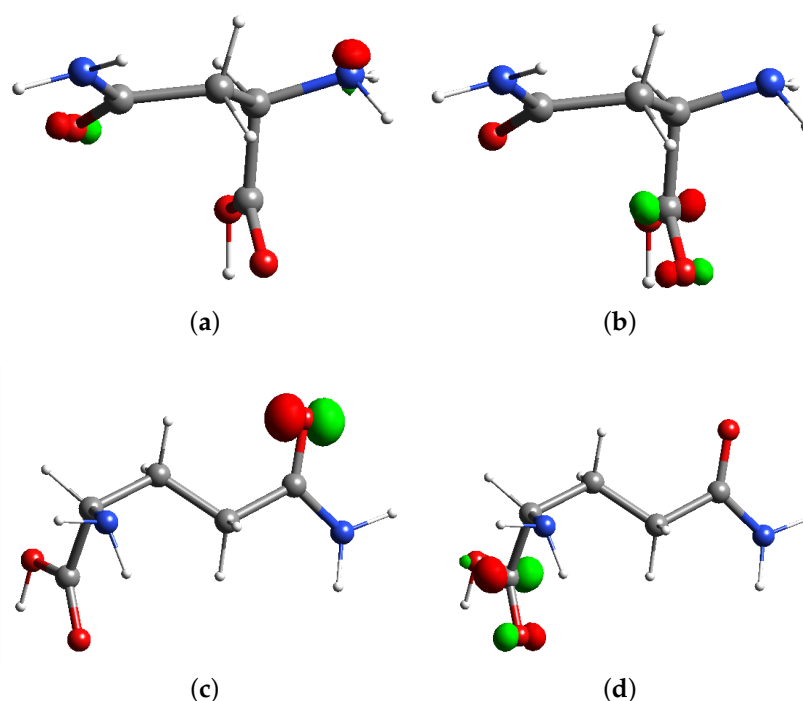


Figure 6. FMO of ASP and GLU. (a) ASP's HOMO (ISO = 0.2); (b) ASP's LUMO (ISO = 0.2); (c) GLU's HOMO (ISO = 0.2); (d) GLU's LUMO (ISO = 0.2).

The analytical Fukui isosurfaces ($f^-(\mathbf{r})$ and $f^+(\mathbf{r})$) of ASP and GLU are shown in Figure 7. Figure 7a,b shows the ASP surface's $f^-(\mathbf{r})$ and $f^+(\mathbf{r})$ plots, respectively. The amine group, which was next to carboxylic acid, acts as an oxidation center, and the carboxylic group acts as a reduction center. Similarly, Figure 7c,d shows the GLU surface's $f^-(\mathbf{r})$ and $f^+(\mathbf{r})$ plots, respectively. The oxygen atom of the acetamide group acts as an oxidation center, and the carboxylic group acts as the reduction center. The FMO results offer data on the redox ET sites without taking electronic relaxation into account. However, the analytical Fukui findings provide information on the redox ET locations while accounting for relaxation effects. Therefore, the FMO and Fukui data should be connected to forecast redox reactivity areas more precisely. Both the FMO and Fukui studies are in agreement with one another in the current research. Therefore, our findings are that the amine group is the oxidation center at ASP, and that the oxygen atom of the acetamide group is the oxidation center at the GLU. In both ASP and GLU, the carboxylic acid group is the reduction center.

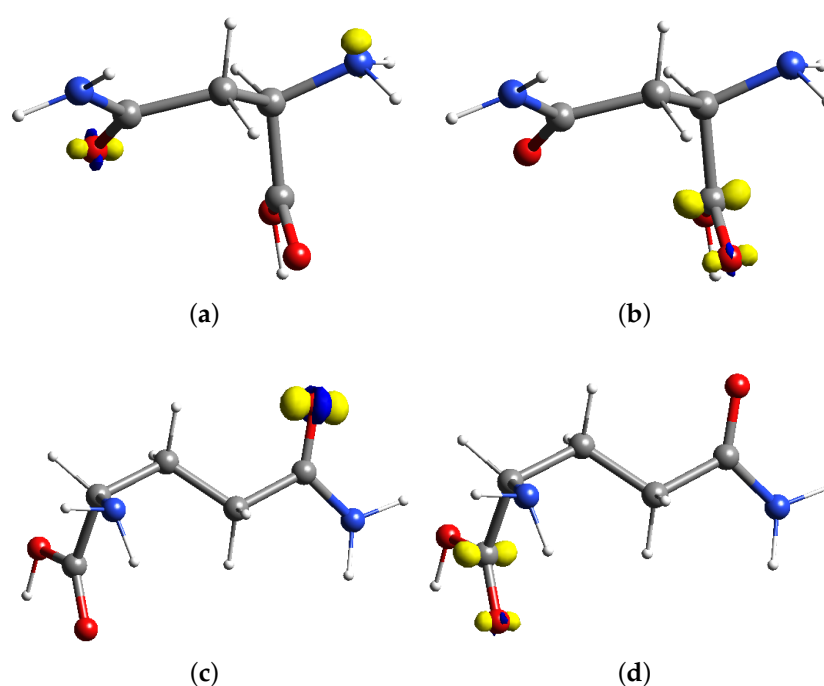


Figure 7. Analytical Fukui of ASP and GLU. (a) $f^-(\mathbf{r})$ (ISO = 0.039); (b) $f^+(\mathbf{r})$ (ISO = 0.045); (c) $f^-(\mathbf{r})$ (ISO = 0.05); (d) $f^+(\mathbf{r})$ (ISO = 0.05).

3.6. Effect of Concentration of DA at ASP-MCPE and GLU-MCPE

The CV method was used to investigate the effect of DA concentration at the surface ASP-MCPE in 0.1 M PBS, pH 7.4. (as shown in Figure 8). The DA concentration was gradually increased from 10 to 30 μM with intervals of 5 μM . The peak current increased linearly as DA concentration increased (inset of Figure 8) according to the following regression equation: $i_{pa} = 0.902c$ (DA concentration in μM) + 0.95216, with an R^2 value of 0.9958.

CVs obtained at the surface of GLU-MCPE in 0.1 M PBS at pH 7.4 are shown in Figure 9. For DA concentrations ranging from 10 to 25 μM at the GLU-MCPE, as the DA concentration rose (each step with a 5 μM increment), the oxidation peak current of DA also rose. The peak current increased linearly as the DA concentration increased (inset of Figure 9) according to the following regression equation: $i_{pa} = 0.902c$ (DA concentration in μM) + 0.95216 with R^2 value 0.9987.

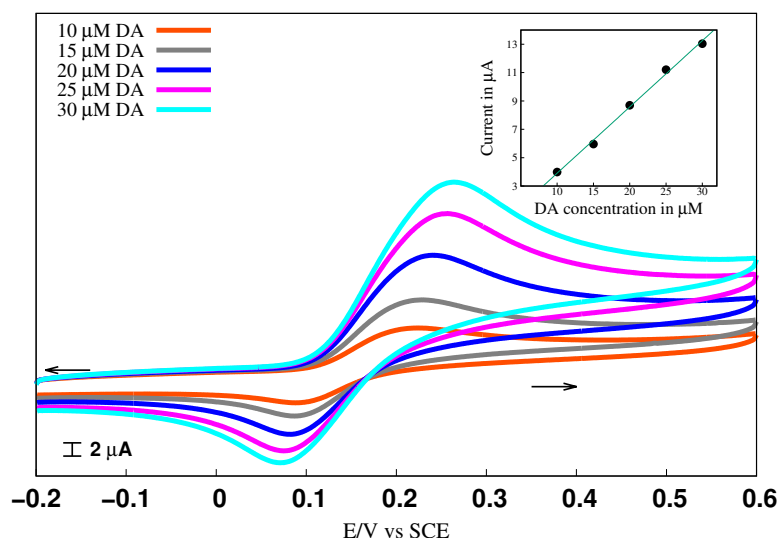


Figure 8. CVs of different DA concentrations at ASP-MCPE in 0.1 M PBS. Inset graph of concentration vs. i_{pa} .

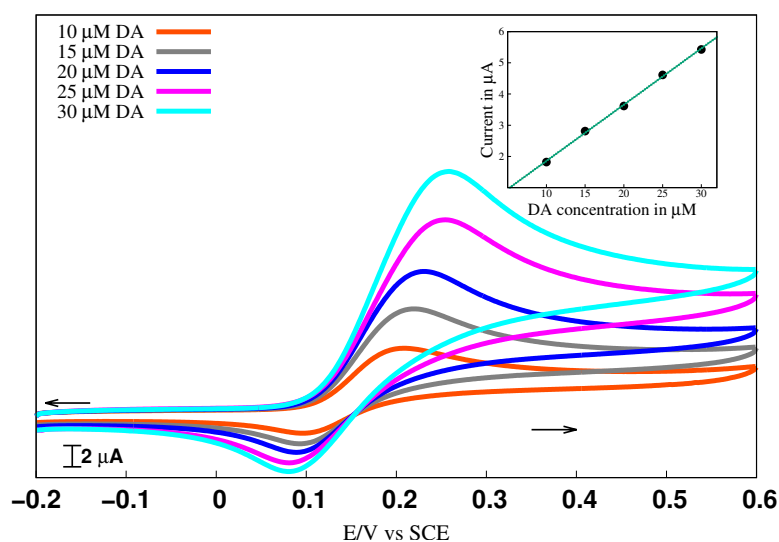


Figure 9. CVs of different DA concentrations at GLU-MCPE in 0.1 M PBS. Inset graph of concentration vs. i_{pa} .

3.7. Determination of DA in Commercial Injection Samples

By determining DA in the DA injection, we evaluated the practical applicability of ASP-MCPE and GLU-MCPE. Sterile Specialities India Pvt Ltd. provided the DA injection sample. With the help of 0.1 M PBS, DA injections were diluted at a 1:25 ratio. Tables 5 and 6 show the results for ASP-MCPE and GLU-MCPE, respectively. The recovery was acceptable for both electrodes, indicating that the ASP-MCPE and GLU-MCPE could be used efficiently for determining DA in commercial injection formulations, with a recovery rate of 99.90–99.5% for ASP-MCPE, and of 99.90–99.6% for GLU-MCPE.

Table 5. Results of DA analysis in real samples with ASP-MCPE.

| SI/No. | DA Spiked (μL) | DA Sensed (μL) | Deviation (μL) | Recovery (%) |
|--------|-----------------------------|-----------------------------|-----------------------------|--------------|
| 1 | 15 | 14.85 | −0.15 | 99.0 |
| 2 | 20 | 19.90 | −0.10 | 99.5 |

Table 6. Results of DA analysis in real samples with GLU-MCPE.

| SI/No. | DA Spiked (μL) | DA Sensed (μL) | Deviation (μL) | Recovery (%) |
|--------|----------------|----------------|----------------|--------------|
| 1 | 20 | 19.80 | −0.20 | 99.0 |
| 2 | 25 | 24.90 | −0.10 | 99.6 |

4. Conclusions

In the present research, the CPE was modified by grinding ASP and GLU (both environmentally friendly modifiers) using a pestle and mortar. ASP displayed a worthy electrocatalytic property on the CPE surface compared to GLU for detecting DA. DA can bind easily on ASP when compared to GLU. In addition, the electron-donating and accepting power of ASP is higher than GLU. Therefore, ASP has a higher electrocatalytic activity than GLU. ASP and GLU have a similar functional group (acetamide, amine, and carboxylic acid). However, the GLU carbonyl carbon atom of the amide group experiences a reduced negative inductive effect from the amine group. Therefore, carbonyl oxygen's lone pair of electrons are easier to remove in the case of GLU when compared to ASP. This may be the reason for the higher electrocatalytic activity of ASP when compared to GLU. Analytical Fukui and FMO were able to discriminate the redox ET regioselectivity at ASP and GLU. As a part of our work, we have also tested the abilities of ASP-MCPE and GLU-MCPE for detecting DA in commercial injection samples. ASP-MCPE and GLU-MCPE showed excellent capabilities, with 99–99.5%. Here, the CV and DFT results are well-concordant in this instance. Therefore, quantum chemical methods can be used to select the electrocatalyst to modify CPE for sensing applications.

Author Contributions: G.K.J.: conceptualization, experimental validation, formal analysis, original draft preparation, and editing; B.E.K.S.: formal analysis and editing; R.F.-M.: resources and editing; K.P.-U.: experimental validation and original draft preparation. All authors have read and agreed to the published version of the manuscript.

Funding: This research was funded by the Department of Sciences and Technology, SERB-TARE SQUID-1989-GJ-4973 (TAR/2021/000197).

Data Availability Statement: Not applicable.

Conflicts of Interest: The authors declare no conflict of interest.

References

- Robinson, D.L.; Hermans, A.; Seipel, A.T.; Wightman, R.M. Monitoring Rapid Chemical Communication in the Brain. *Chem. Rev.* **2008**, *108*, 2554–2584. [[CrossRef](#)] [[PubMed](#)]
- Herlenius, E.; Lagercrantz, H. Development of neurotransmitter systems during critical periods. *Exp. Neurol.* **2004**, *190*, 8–21. [[CrossRef](#)] [[PubMed](#)]
- Antonelli, F.; Strafella, A.P. Behavioral disorders in Parkinson's disease: The role of dopamine. *Park. Relat. Disord.* **2014**, *20*, S10–S12. [[CrossRef](#)] [[PubMed](#)]
- Ba, F.; Martin, W.W. Dopamine transporter imaging as a diagnostic tool for parkinsonism and related disorders in clinical practice. *Park. Relat. Disord.* **2015**, *21*, 87–94. [[CrossRef](#)]
- Kim, J.; Jeon, M.; Paeng, K.J.; Paeng, I.R. Competitive enzyme-linked immunosorbent assay for the determination of catecholamine, dopamine in serum. *Anal. Chim. Acta* **2008**, *619*, 87–93. [[CrossRef](#)]
- Lin, Y.; Chen, C.; Wang, C.; Pu, F.; Ren, J.; Qu, X. Silver nanoprobe for sensitive and selective colorimetric detection of dopamine via robust Ag–catechol interaction. *Chem. Commun.* **2011**, *47*, 1181–1183. [[CrossRef](#)]
- Qin, W.W.; Wang, S.P.; Li, J.; Peng, T.H.; Xu, Y.; Wang, K.; Shi, J.Y.; Fan, C.H.; Li, D. Visualizing dopamine released from living cells using a nanoplasmonic probe. *Nanoscale* **2015**, *7*, 15070–15074. [[CrossRef](#)]
- Olefirowicz, T.M.; Ewing, A.G. Dopamine concentration in the cytoplasmic compartment of single neurons determined by capillary electrophoresis. *J. Neurosci. Methods* **1990**, *34*, 11–15. [[CrossRef](#)]
- Adkins, E.M.; Samuvel, D.J.; Fog, J.U.; Eriksen, J.; Jayanthi, L.D.; Vaegter, C.B.; Ramamoorthy, S.; Gether, U. Membrane Mobility and Microdomain Association of the Dopamine Transporter Studied with Fluorescence Correlation Spectroscopy and Fluorescence Recovery after Photobleaching. *Biochemistry* **2007**, *46*, 10484–10497. [[CrossRef](#)]

10. An, J.H.; Choi, D.K.; Lee, K.J.; Choi, J.W. Surface-enhanced Raman spectroscopy detection of dopamine by DNA Targeting amplification assay in Parkinson's model. *Biosens. Bioelectron.* **2015**, *67*, 739–746. [[CrossRef](#)]
11. Jauhar, S.; McCutcheon, R.; Borgan, F.; Veronese, M.; Nour, M.; Pepper, F.; Rogdaki, M.; Stone, J.; Egerton, A.; Turkheimer, F.; et al. The relationship between cortical glutamate and striatal dopamine in first-episode psychosis: A cross-sectional multimodal PET and magnetic resonance spectroscopy imaging study. *Lancet Psychiatry* **2018**, *5*, 816–823. [[CrossRef](#)] [[PubMed](#)]
12. Pettingill, T.; Strange, R.; Blackburn, N. Carbonmonoxy dopamine beta-hydroxylase. Structural characterization by Fourier transform infrared, fluorescence, and X-ray absorption spectroscopy. *J. Biol. Chem.* **1991**, *266*, 16996–17003. [[CrossRef](#)] [[PubMed](#)]
13. Jayaprakash, G.K.; Swamy, B.E.K.; Casillas, N.; Flores-Moreno, R. Analytical Fukui and cyclic voltammetric studies on ferrocene modified carbon electrodes and effect of Triton X-100 by immobilization method. *Electrochim. Acta* **2017**, *258*, 1025–1034. [[CrossRef](#)]
14. Jayaprakash, G.K.; Swamy, B.E.K.; Chandrashekar, B.N.; Flores-Moreno, R. Theoretical and cyclic voltammetric studies on electrocatalysis of benzethonium chloride at carbon paste electrode for detection of dopamine in presence of ascorbic acid. *J. Mol. Liq.* **2017**, *240*, 395–401. [[CrossRef](#)]
15. Jayaprakash, G.K.; Kumara Swamy, B.; Rajendrachari, S.; Sharma, S.; Flores-Moreno, R. Dual descriptor analysis of cetylpyridinium modified carbon paste electrodes for ascorbic acid sensing applications. *J. Mol. Liq.* **2021**, *334*, 116348. [[CrossRef](#)]
16. Kudur Jayaprakash, G.; Kumara Swamy, B.E.; Nicole González Ramírez, H.; Tumbre Ekanthappa, M.; Flores-Moreno, R. Quantum chemical and electrochemical studies of lysine modified carbon paste electrode surfaces for sensing dopamine. *New J. Chem.* **2018**, *42*, 4501–4506. [[CrossRef](#)]
17. Kudur Jayaprakash, G.; Kumara Swamy, B.E.; Sharma, S.; Santoyo-Flores, J.J. Analyzing electron transfer properties of ferrocene in gasoline by cyclic voltammetry and theoretical methods. *Microchem. J.* **2020**, *158*, 105116. [[CrossRef](#)]
18. Kalcher, K. Chemically modified carbon paste electrodes in voltammetric analysis. *Electroanalysis* **1990**, *2*, 419–433. [[CrossRef](#)]
19. Švancara, I.; Vytrás, K.; Kalcher, K.; Walcarius, A.; Wang, J. Carbon Paste Electrodes in Facts, Numbers, and Notes: A Review on the Occasion of the 50-Years Jubilee of Carbon Paste in Electrochemistry and Electroanalysis. *Electroanalysis* **2009**, *21*, 7–28. [[CrossRef](#)]
20. Wang, J.; Naser, N.; Angnes, L.; Wu, H.; Chen, L. Metal-dispersed carbon paste electrodes. *Anal. Chem.* **1992**, *64*, 1285–1288. [[CrossRef](#)]
21. Švancara, I.; Vytrás, K.; Barek, J.; Zima, J. Carbon Paste Electrodes in Modern Electroanalysis. *Crit. Rev. Anal. Chem.* **2001**, *31*, 311–345. [[CrossRef](#)]
22. Winiarski, J.P.; Tavares, B.F.; de Fátima Ulbrich, K.; de Campos, C.E.M.; Souza, A.A.; Souza, S.M.G.U.; Jost, C.L. Development of a multianalyte electrochemical sensor for depression biomarkers based on a waste of the steel industry for a sustainable and one-step electrode modification. *Microchem. J.* **2022**, *175*, 107141. [[CrossRef](#)]
23. Decarli, N.O.; Zapp, E.; de Souza, B.S.; Santana, E.R.; Winiarski, J.P.; Vieira, I.C. Biosensor based on laccase-halloysite nanotube and imidazolium zwitterionic surfactant for dopamine determination. *Biochem. Eng. J.* **2022**, *186*, 108565. [[CrossRef](#)]
24. Jayaprakash, G.K.; Flores-Moreno, R.; Swamy, B.E.K.; Mohanty, K.; Dhiman, P. Pre/post electron transfer regioselectivity at glycine modified graphene electrode interface for voltammetric sensing applications. *J. Electrochem. Sci. Eng.* **2022**, *12*, 1001–1008. [[CrossRef](#)]
25. Kumar, R.S.; Jayaprakash, G.K.; Manjappa, S.; Kumar, M.; Kumar, A.P. Theoretical and electrochemical analysis of L-serine modified graphite paste electrode for dopamine sensing applications in real samples. *J. Electrochem. Sci. Eng.* **2022**, *12*, 1243–1250. [[CrossRef](#)]
26. de Fatima Ulbrich, K.; Winiarski, J.P.; Jost, C.L.; Maduro de Campos, C.E. Mechanochemical synthesis of a Ni₃-xTe₂ nanocrystalline composite and its application for simultaneous electrochemical detection of dopamine and adrenaline. *Compos. Part B Eng.* **2020**, *183*, 107649. [[CrossRef](#)]
27. Zamarchi, F.; Silva, T.R.; Winiarski, J.P.; Santana, E.R.; Vieira, I.C. Polyethylenimine-Based Electrochemical Sensor for the Determination of Caffeic Acid in Aromatic Herbs. *Chemosensors* **2022**, *10*, 357. [[CrossRef](#)]
28. Flores-Álvarez, J.; Cortés-Arriagada, D.; Reyes-Gómez, J.; Gómez-Sandoval, Z.; Rojas-Montes, J.; Pineda-Urbina, K. 2-Mercaptobenzothiazole modified carbon paste electrode as a novel copper sensor: An electrochemical and computational study. *J. Electroanal. Chem.* **2021**, *888*, 115208. [[CrossRef](#)]
29. Estrada-Aldrete, J.; Hernández-López, J.; García-León, A.; Peralta-Hernández, J.; Cerino-Córdova, F. Electroanalytical determination of heavy metals in aqueous solutions by using a carbon paste electrode modified with spent coffee grounds. *J. Electroanal. Chem.* **2020**, *857*, 113663. [[CrossRef](#)]
30. Zhang, Y.; Zheng, J.B. Comparative investigation on electrochemical behavior of hydroquinone at carbon ionic liquid electrode, ionic liquid modified carbon paste electrode and carbon paste electrode. *Electrochim. Acta* **2007**, *52*, 7210–7216. [[CrossRef](#)]
31. Tajik, S.; Beitollahi, H.; Nejad, F.G.; Safaei, M.; Zhang, K.; Van Le, Q.; Varma, R.S.; Jang, H.W.; Shokouhimehr, M. Developments and applications of nanomaterial-based carbon paste electrodes. *RSC Adv.* **2020**, *10*, 21561–21581. [[CrossRef](#)] [[PubMed](#)]
32. Vajdle, O.; Šekuljica, S.; Guzsvány, V.; Nagy, L.; Kónya, Z.; Avramov Ivić, M.; Mijin, D.; Petrović, S.; Anojić, J. Use of carbon paste electrode and modified by gold nanoparticles for selected macrolide antibiotics determination as standard and in pharmaceutical preparations. *J. Electroanal. Chem.* **2020**, *873*, 114324. [[CrossRef](#)]

33. Kummari, S.; Sunil Kumar, V.; Yugender Goud, K.; Vengatajalabathy Gobi, K. Nano-Au particle decorated poly-(3-amino-5-hydroxypyrazole) coated carbon paste electrode for in-vitro detection of valacyclovir. *J. Electroanal. Chem.* **2022**, *904*, 115859. [[CrossRef](#)]
34. Martínez, J. Local reactivity descriptors from degenerate frontier molecular orbitals. *Chem. Phys. Lett.* **2009**, *478*, 310–322. [[CrossRef](#)]
35. Morell, C.; Grand, A.; Toro-Labbé, A. Theoretical support for using the $\Delta f(r)$ descriptor. *Chem. Phys. Lett.* **2006**, *425*, 342–346. [[CrossRef](#)]
36. Martínez-Araya, J.I. Why is the dual descriptor a more accurate local reactivity descriptor than Fukui functions? *J. Math. Chem.* **2015**, *53*, 451–465. [[CrossRef](#)]
37. Jayaprakash, G.K. Pre-post redox electron transfer regioselectivity at the alanine modified nano graphene electrode interface. *Chem. Phys. Lett.* **2022**, *789*, 139295. [[CrossRef](#)]
38. Barrera, Y.; Anderson, J.S. Predicting the reactivity of unsaturated molecules to methyl radical addition using a radical two-parameter general-purpose reactivity indicator. *Chem. Phys. Lett.* **2022**, *791*, 139333. [[CrossRef](#)]
39. Jayaprakash, G.K.; Flores-Moreno, R. Regioselectivity in hexagonal boron nitride co-doped graphene. *New J. Chem.* **2018**, *42*, 18913–18918. [[CrossRef](#)]
40. Zhu, M.; Li, R.; Lai, M.; Ye, H.; Long, N.; Ye, J.; Wang, J. Copper nanoparticles incorporating a cationic surfactant-graphene modified carbon paste electrode for the simultaneous determination of gatifloxacin and pefloxacin. *J. Electroanal. Chem.* **2020**, *857*, 113730. [[CrossRef](#)]
41. Flores-Moreno, R.; Pineda-Urbina, K.; Gómez-Sandoval, Z. *Sinapsis, Version XII-V*; Sinapsis Developers: Buenos Aires, Argentina, 2012.
42. Geudtner, G.; Calaminici, P.; Carmona-Espíndola, J.; del Campo, J.M.; Domínguez-Soria, V.D.; Moreno, R.F.; Gamboa, G.U.; Goursot, A.; Köster, A.M.; Reveles, J.U.; et al. deMon2k. *WIREs Comput. Mol. Sci.* **2012**, *2*, 548–555. [[CrossRef](#)]
43. Flores-Moreno, R.; Köster, A.M. Auxiliary density perturbation theory. *Chem. Phys.* **2008**, *128*, 134105. [[CrossRef](#)] [[PubMed](#)]
44. Lee, C.; Yang, W.; Parr, R.G. Development of the Colle-Salvetti correlation-energy formula into a functional of the electron density. *Phys. Rev. B* **1988**, *37*, 785–789. [[CrossRef](#)] [[PubMed](#)]
45. Becke, A.D. Density-functional exchange-energy approximation with correct asymptotic behavior. *Phys. Rev. A* **1988**, *38*, 3098–3100. [[CrossRef](#)] [[PubMed](#)]
46. Godbout, N.; Salahub, D.R.; Andzelm, J.; Wimmer, E. Optimization of Gaussian-Type Basis Sets for Local Spin Density Functional Calculations. Part I. Boron through Neon, Optimization Technique and Validation. *Can. J. Chem.* **1992**, *70*, 560–571. [[CrossRef](#)]
47. Pearlman, D.A.; Case, D.A.; Caldwell, J.W.; Ross, W.S.; Cheatham, T.E.; DeBolt, S.; Ferguson, D.; Seibel, G.; Kollman, P. AMBER, a package of computer programs for applying molecular mechanics, normal mode analysis, molecular dynamics and free energy calculations to simulate the structural and energetic properties of molecules. *Comput. Phys. Commun.* **1995**, *91*, 1–41. [[CrossRef](#)]
48. Allouche, A.R. Gabedit—A graphical user interface for computational chemistry softwares. *J. Comput. Chem.* **2011**, *32*, 174–182. [[CrossRef](#)]
49. Rodríguez, A.; Rodríguez-Fernández, R.; A. Vázquez, S.; L. Barnes, G.; Stewart, J.J.P.; Martínez-Núñez, E. tsscads2018: A code for automated discovery of chemical reaction mechanisms and solving the kinetics. *J. Comput. Chem.* **2018**, *39*, 1922–1930. [[CrossRef](#)]
50. Neese, F. The ORCA program system. *WIREs Comput. Mol. Sci.* **2012**, *2*, 73–78. [[CrossRef](#)]

Disclaimer/Publisher’s Note: The statements, opinions and data contained in all publications are solely those of the individual author(s) and contributor(s) and not of MDPI and/or the editor(s). MDPI and/or the editor(s) disclaim responsibility for any injury to people or property resulting from any ideas, methods, instructions or products referred to in the content.